applied sciences

MDPI

Article

Comparative Assessment of Variable Loads and Seismic Actions on Bridges: A Case Study in Italy Using a Multimodal Approach

Daniele Collura and Roberto Nascimbene *

Istituto Universitario di Studi Superiori—IUSS, Scuola Universitaria Superiore IUSS, 27100 Pavia, Italy
* Correspondence: roberto.nascimbene@iusspavia.it

Abstract: The structural safety of the infrastructure stock is an important issue in modern seismic performance assessments. Following recent seismic events, reports have highlighted the increased vulnerability of physical infrastructural assets, particularly for many bridges across the Italian road and motorway network. Italy possesses one of the most complex and intricate road systems in Europe which was constructed across irregular territories in terms of plan and elevation and of varying dimensions. As such, a comparative case study is presented herein. This case study aims to characterise the seismic vulnerability of the Vizzana-Zampogna viaduct which is part of the A15 Parma-La Spezia motorway, near the locality of Selva Bocchetto. The viaduct is considered representative of the 1970s construction period. It is approximately 342 m in length and is characterized by a flat curvilinear prestressed concrete deck consisting of 15 spans simply supported on reinforced concrete piers. To better understand the seismic structural response of the individual piers of the viaduct, a "multi-modal" nonlinear static analysis was developed, which allows the effects of sectional stresses relative to the variable load profiles of the single modes to be combined through the quadratic modal combination, and to be compared with the relevant limit state. The research aims to qualitatively identify the piers most vulnerable to seismic action and to study the effects that are induced by introducing variable loads and intensity scenarios of different earthquakes.

Keywords: highway bridges; numerical study; seismic performance; existing bridge; finite element modelling

Citation: Collura, D.; Nascimbene, R. Comparative Assessment of Variable Loads and Seismic Actions on Bridges: A Case Study in Italy Using a Multimodal Approach. *Appl. Sci.* **2023**, *13*, 2771. https://doi.org/10.3390/app13052771

Academic Editors: Jong Wan Hu and Junwon Seo

Received: 26 January 2023
Revised: 17 February 2023
Accepted: 19 February 2023
Published: 21 February 2023

1. Introduction

Recent earthquakes have highlighted the vulnerability of bridges and highway infrastructures in areas of medium to high seismicity [1–4]. In the past, infrastructure networks and particularly bridges were constructed before the introduction of modern European and International seismic standards [5–9]. As such, existing bridges are characterized by an increased vulnerability to earthquake ground-shaking events [10–15]. Furthermore, in Italy, the critical condition of ageing infrastructure has recently received international attention due to the recent collapse of the Morandi bridge [16,17] and other infrastructures [18]. For the mitigation of further physical, human and economic loss, a proper vulnerability assessment coupled with the identification of adequate retrofitting strategies for the structural system should be carried out [19–23]. Recently, experimental campaigns highlighted the effectiveness of seismic isolation as a major retrofitting technique for damage prevention in reinforced concrete piers. This is due especially to limiting the maximum base shear at the base of the piers, decreasing the lateral drifts, and preventing the onset of inelastic deformation in the frame sections [24,25]. Furthermore, significant residual drifts sustained following earthquake events render concrete bridge piers more vulnerable to strong ground motions, subsequently reducing the overall seismic resilience of the infrastructure network. A broad range of mitigation techniques is presented in the literature to reduce the vulnerability of bridge piers located in high seismic zones. After a numerical procedure, many retrofitting techniques can be designed and applied.

Moreover, the overall seismic performance assessment of bridges is a critical research topic of paramount importance. Fragility functions are typically the end result of vulnerability assessment and are inherently governed by quantities subject to numerous sources of both aleatory and epistemic variables, such as modelling uncertainties and record-to-record variability, for example. Much literature highlighted advanced [26,27] or simplified [28–30] methodologies for the aim of carrying out fragility assessment on infrastructure networks. Commonly, when actual bridge damage and ground motion data or the full geometrical properties of the stock are unavailable (or are partially so), analytical fragility curves are used to evaluate highway bridge performance. Furthermore, to improve the ability of numerical models to capture the static and dynamic behaviours of bridges, advanced finite element models were calibrated based on empirical data derived from tests and real-time monitoring techniques applied to existing bridges [31–33]. In many applications, analytical fragility functions also derived from simplified approaches [34,35], and were compared to existing empirical fragility functions to highlight which direction of the bridge was more prominent or vulnerable to vertical and/or horizontal excitation effects [36,37]. Additionally, nonlinear dynamic effects on bridges can affect the ultimate limit state behaviours of the bridge by amplifying the maximum stresses experienced by its different members. Furthermore, risk assessment plays an important role in quantifying earthquake loss and has been widely used in the field of bridge design and seismic engineering [38–40]. However, current studies of risk assessment rarely consider the different variable loads and seismic actions on piers. To this end, this study develops a multi-modal approach for the comparative assessment of variable loads and seismic actions applied to bridges. The multi-modal procedure is presented and applied to an existing 342 m long bridge in Italy, namely the Vizzana-Zampogna viaduct of the A15 Parma-La Spezia motorway (central part of Italy).

2. Case Study Description

The Vizzana-Zampogna viaduct of the CISA motorway A15 (Parma–La Spezia) is located in Central Italy and is a structural system consisting of two distinct roadways, formed respectively by fifteen spans on the northern side, and sixteen spans on the southern side. The aforementioned case-study bridge is shown in Figure 1.

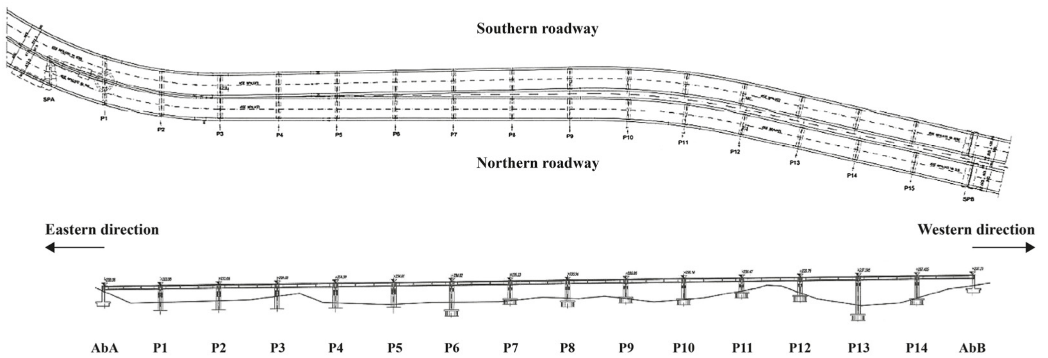

Figure 1. Elevation and plan view of the case study Vizzana-Zampogna viaduct located in central Italy.

The spans are isostatic with a beam pattern, resting on piles and abutments in reinforced concrete. The plan view layout has a curvilinear trend, as shown in Figure 1.

The spans have a longitudinal distance between the supports of 22.80 m and are made up of four "I-shaped" beams with a transverse distance of 2.48 m and a height of 1.40 m. The prestressed concrete beams are connected by four transverse beams; the prestress action is obtained by the application of seventy-two pre-tensioned strands ϕ = 5/16 and one single post-tensioned cable with 18 wires ϕ = 7 mm. The slab has a total mean thickness of 0.22 m and was partially cast on-site between AbA (abutment A in Figure 1) and P3 (Pile 3). The net width of the carriageway is nearly constant at about 8.1 m.

The reinforced concrete piles consist of two vertical walls 0.70 m thick, linked at the top by a horizontal reinforced concrete beam of 0.50 m. The width of the walls varies between the P1–P6 piles, supporting both carriageways, whereas it is constant on the remaining piles. The bridge foundations are of the "shaft" type and will not be considered in the finite element model. Hence, soil-structure interactions will not be investigated since that is not the main goal of this study. As such, piers are considered fully fixed to the ground. The supports at the top of the piers consist of reinforced neoprene with dimensions of 200 mm × 400 mm × 41 mm. The stratigraphy is composed of four layers of steel sheet with a thickness of 3 mm, and three internal layers of 8 mm rubber for an overall height of 41 mm.

3. Seismic Input, Load Scenarios and Analyses

The current Italian regulations (NTC 2018) [41] infer that masses associated with verified traffic loads should not be considered in the seismic load combination. As such, the considered model accounts only for combined vertical loads due to self-weights associated with structural and non-structural elements: G1 + G2 (hereinafter called "scenario A"). In any case, the purpose of this research is to investigate the structural behaviour of the viaduct subjected to a more critical scenario given the strategic nature of the bridge under consideration. Subsequently, an alternative vertical load scenario (termed "scenario B") was defined, in which the traffic and seismic loads were considered in the load combination rule for the ultimate limit state (ULS or collapse prevention). In other words, the assumed traffic scenario is of stationary vehicles (i.e., in a queue or tailback), considered as seismic load in the design with regard to a life-safety ultimate limit state (or SLV [41]). Therefore, in the next section, a finite element model was developed in which the vertical traffic loads will also be present ("scenario B") according to the provisions at point 5.1.3 in [41], and briefly reported in Table 1 (values were reported per unit length corresponding to a 1 m strip of deck). Traffic loads were modelled as uniformly distributed loads by summing the contribution of concentrated and distributed loads as per the Italian legislation (Table 1). These uniform loads were applied to the case study bridge along the barycentric axis of the beam elements that will make up the modelling of the deck as outlined in Section 4.

Table 1. Vertical load analysis of the viaduct. The table shows the conventional calculation of traffic loads that will be applied to the viaduct model in load scenario B.

<table>
<tr><td rowspan="2">GEOMETRY</td><th>Slab Width [m]</th><th>Conventional IT Code Lanes</th><th>Length L [m]</th><th>L Remaining [m]</th></tr>
<tr><td>8.12</td><td>2</td><td>3</td><td>2.12</td></tr>
<tr><td rowspan="4">LOADS</td><th>Conventional IT Code Lane</th><th>Concentrated Loads [kN/m]</th><th colspan="2">Distributed Loads [kN/m^2 × m]</th></tr>
<tr><td>1</td><td>300</td><td colspan="2">27</td></tr>
<tr><td>2</td><td>200</td><td colspan="2">7.5</td></tr>
<tr><td>remaining</td><td>0</td><td colspan="2">5.3</td></tr>
<tr><th colspan="2">Total loads</th><td>500</td><td colspan="2">39.8</td></tr>
</table>

As highlighted in Table 1, vertical loads of the slab yield a total weight of 539.8 kN/m applied on the deck, which are assumed to be reduced by the combination coefficient $\Psi_{2,k}$ = 0.2 and resulting in a weight of 107.96 kN/m, to be applied on the northern and southern spans of the viaduct (Figure 1). In addition, four seismic inputs were defined for the two different analyses carried out: two for nonlinear static analysis (NLSA) and two for nonlinear dynamic analysis (NLDA).

3.1. Nonlinear-Static Analysis (NLSA—Multimodal Pushover Analysis or MMPO)

In the framework of the NLSA, two principal horizontal seismic motion input corresponding to two load cases were introduced: n. 1 based on the Italian National code [41] non-site-specific spectrum (NSS) approach, and n. 2 using a site-specific spectrum (SSS) approach.

Considering the first input seismic motion, it is quite important to highlight that the viaduct is entirely an infrastructure pertaining to the then-administrative department of the municipality of Terenzo (Parma). The Italian update of the seismic classification of the Emilia-Romagna region relocates the territory of the municipality of Terenzo to seismic zone 3 following the most recent classification of seismic hazard. This corresponds to a maximum acceleration expected on the ground (with a probability of exceeding 10% in 50 years) between 0.05 g and 0.15 g: the viaduct seismic ground acceleration is a_{gSLV} (T_r = 50 years) = 0.069 g.

To define the design spectrum, it is necessary to investigate the soil on which the viaduct is located. Official documentation, made available by the Emilia-Romagna region, indicate that the main stratigraphic characteristics of the soils of the municipality are remarkably heterogeneous, with V_{sH} (shear wave velocity) ranging between 202 m/s and 559 m/s. However, this research additionally benefitted from some MASW (multichannel analysis of surface waves) seismic tests carried out, one of which was performed in the vicinity of the A15 motorway in a section adjacent to the viaduct. A value of the shear velocity V_{sH} = 225 m/s was reported which suggests characterising the site as a type C subsoil as per the Italian design code [41]. To be on the conservative side of this approach, the topographical effects of the site were also considered, observing that the motorway viaduct is located along the ridge of a slope that ends in the bed of the Taro River. For this reason, a S_T value of 1.2 (topographic category T_2, h/H = 0.5) was assumed. Table 2 outlines the spectral parameters of the elastic response spectrum, and Figure 2 illustrates a comparison between the elastic response spectrum of soil type A and the elastic response spectrum of the Terenzo site for ULS according to the Italian design code [41].

With regards to horizontal load case n. 2 corresponding to the SSS approach, the Emilia-Romagna Region, generally, and the municipality of Terenzo (i.e., the territory within which the viaduct is located), specifically, have consistently remained within a level 2 seismic zone following a regional seismic micro-zonation study conducted in 2017 [42]. In particular, 36 single-station seismic tests (HVSR—Horizontal to Vertical Spectral Ratio Analysis) and 14 geophysical surveys of the MASW + HVSR type were performed and 11 geo-mechanical surveys were also carried out on outcrops belonging to the various formations present in the municipal area.

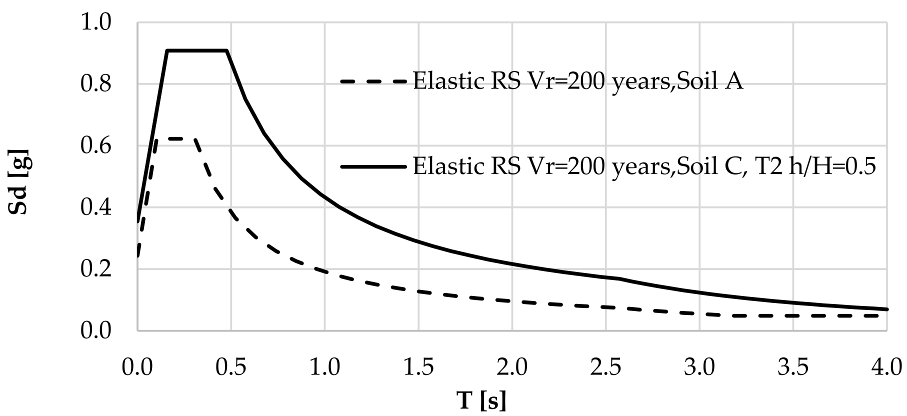

Figure 2. Comparison between elastic response spectrum for soil A and elastic response spectrum for the Terenzo site for ULS, according to Italian the design code.

Table 2. Implemented parameters for the national spectrum in the design code. Benchmarks of the Terenzo site (ULS, Vr = 200 years, Soil type C, topography T_2).

Input Parameters						
a_g	F_0	T_c*	S_s	C_c	S_t	q
0.243	2.560	0.307	1.327	1.550	1.100	1.000
Output Parameters						
S	η	T_b	T_c	T_d		
1.459	1.000	0.159	0.476	2.573		

Table 3 and Figure 3 [42] illustrate the velocity of the shear waves β at various depths and the thickness of the layer H with homogenous shear wave velocities, measured with an HVSR test near the viaduct in Selva Bocchetto zone (Terenzo, PR—Parma). According to the measurements of the HVRS test and based on a simplified Italian National Code approach [41], the stratigraphic profile of the Selva Bocchetto site can be associated with an "E" type subsoil, characterized by very low shear wave velocities and a maximum bedrock depth of 30 m (in this case, 8 m).

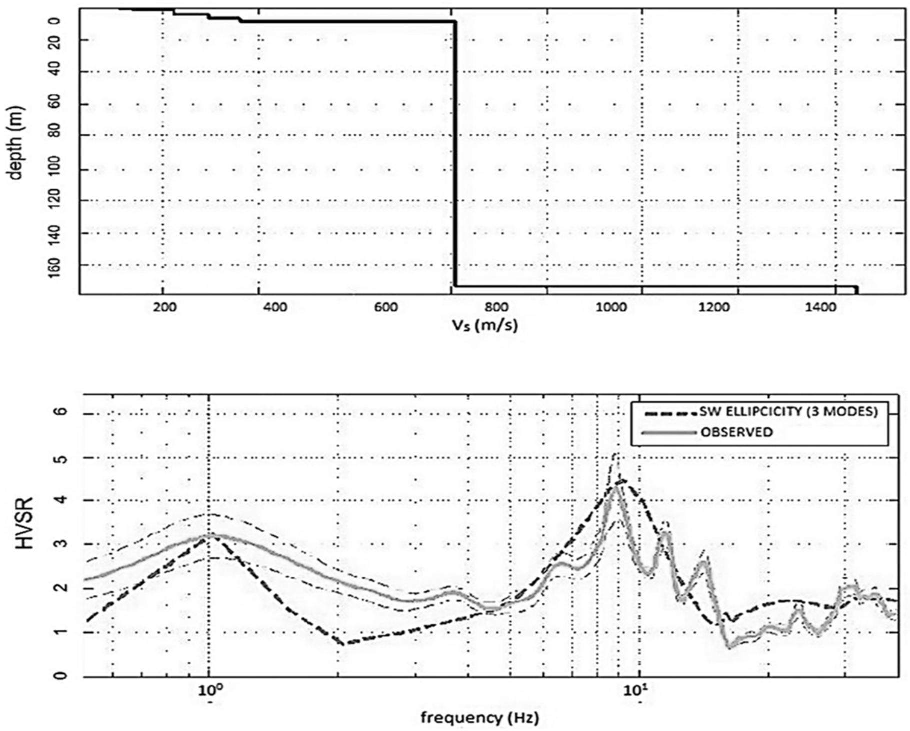

Figure 3. Illustration of the geotechnical stratigraphic profile near the Vizzana-Zampogna viaduct highlighted in [42].

Hence, it seems fully justified to proceed with an evaluation of the amplification of the seismic signal from the bedrock to the surface and, therefore, build a site-specific spectrum. To do this, a soil model was defined using Deepsoil® software [43] by implementing the aforementioned stratigraphy. As a first step, to better understand the evolution of the amplification phenomenon, the fundamental frequency of the stratigraphy can be estimated using the following formula (in agreement with Table 3):

$$\frac{\sum_i^n h_i \cdot \beta_i}{4 \cdot H^2} = 7.79 \text{ Hz}$$

where h_i is the thickness of the i-layer, β_i is the shear velocity of the i-layer and H is the total thickness of the stratigraphic profile over the bedrock (173.4 m).

Table 3. HVSR results at Selva Bocchetto, near the case study viaduct, in terms of shear wave velocities and depths.

Depth [m]		Shear Wave Velocity (β) [m/s]	Thickness of Layer (H) [m]
From	**To**		
0	0.5	78	0.5
0.5	1	138	0.5
1	4.2	224	3.2
4.2	6.4	296	2.2
6.4	8.4	362	2
8.4	173.4	810	165
173.4	infinite	1645	infinite

To understand the post-elastic behaviour of soils, an equivalent linear analytical approach with solutions in the frequency domain was adopted. As clearly known, under the effect of dynamic stresses, soil tends to soften. This effect is expressed according to the hypothesis of a linear-equivalent soil model in terms of the maximum elastic shear stiffness, G_{max}. As the ratio G/G_{max} decreases with the increase in cyclic seismic shear strain, an increase in the soil damping ratio is observed. Consequently, for the calibration of the decay of stiffnesses G/G_{max} and the progressive increase in damping (%) as a function of the displacements of the ground, reference will be made to the seismic micro-zonation study that frames the lithostratigraphic column (mainly gravel-type) of Selva Bocchetto (see Figure 4, where the mean curves of Seed and Idriss [44] are also built and depicted for each soil layer).

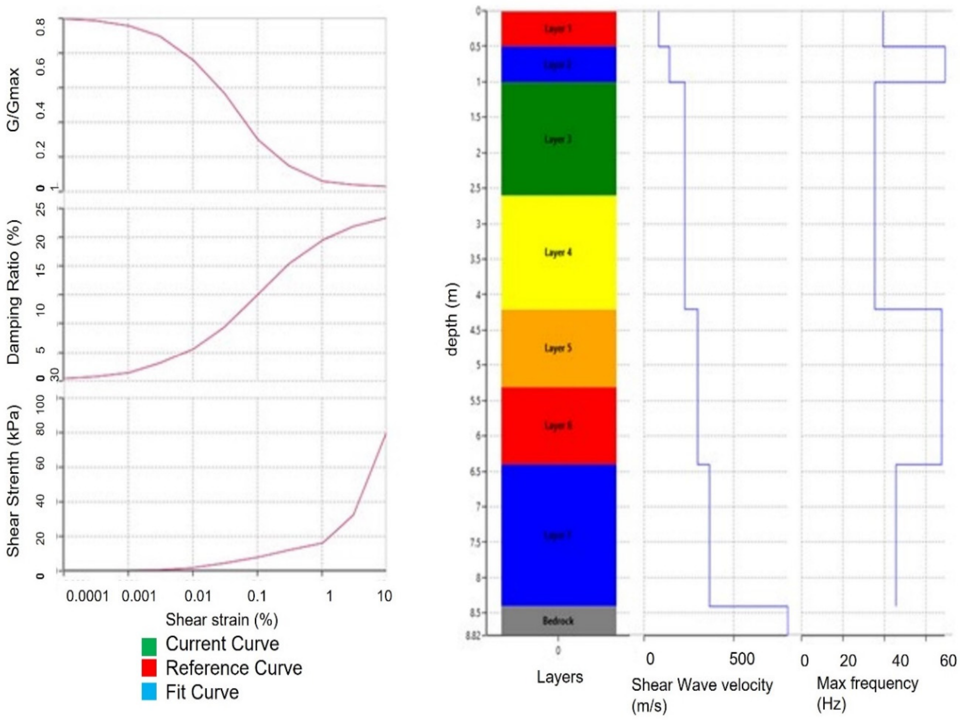

Figure 4. G/Gmax, damping ratio (%) and shear strength (kPa) curves according to Seed and Idriss (1970) (**left**); and the stratigraphic profile model implemented in DeepSoil software and relative shear wave velocity (m/s) (**right**).

The procedure for the derivation of a site-specific spectrum can be summarized as follows:

1. calculation of the response spectra of the input selected accelerograms (seven in total);

2. application of the local seismic response analysis (soil layer response) through the modelling carried out (Figure 4);
3. calculation of the response spectra of the output accelerograms related to the surface soil layer response;
4. calculation of the spectral amplification factors for discrete points (as the period T varies) relative to the same accelerogram, $\frac{Sa_{Surface}}{Sa_{Bedrock}}$;
5. calculation of the mean of the amplification factors (for each single period T) relative to the seven accelerograms;
6. calculation of the code response spectrum on rock (cat. A, according to [41]) magnified with respect to the amplification factors of the single value of T (for discrete periods) calculated above in step 5;
7. regularization of the spectrum obtained according to well-known procedures present in the literature [45–47].

The results obtained are shown in Figure 5 where it is clear how the newly calculated site-specific response spectrum (SSRS) not only results in larger values than (about double) the ones corresponding to the spectrum of the code for subsoil category "E" (IT code response spectrum with the most penalizing spectral accelerations), but the horizontal "plateau" is also shifted towards high frequencies, (potentially) enhancing the contributions of superior modes.

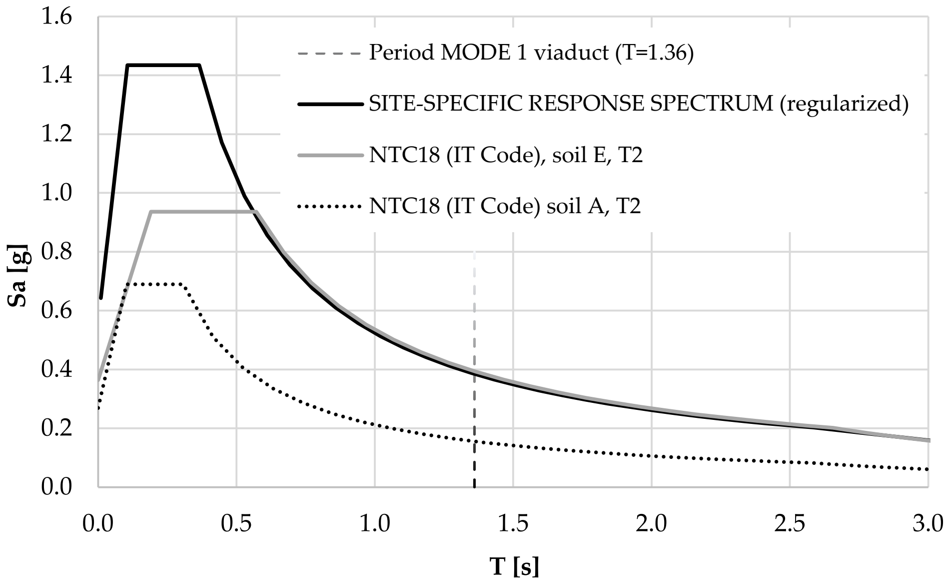

Figure 5. Graphic results of SSRS calculation according to the procedure described through seven steps.

3.2. *Nonlinear-Dynamic Analysis (NLDA)—Time History Analysis*

Nonlinear dynamic analysis consists in computing the seismic response of a structure following a step-wise integration of the equation of motion. This was performed following the application of ground-motion time-histories to a nonlinear model of the structure as will be defined in the present section. To carry out this type of analysis, it is necessary to use nonlinear models that are able to reproduce the post-elastic behaviour of the structural elements in order to accurately represent their dissipative capacity due to hysteresis. In the present case, the nonlinear elements introduced were identified in the plastic hinges modelled at the base of the piers to simulate the post-elastic behaviour of the bridge. For investigating the behaviour of the viaduct, a simplified kinematic-kinetic rule was adopted to define the plastic hinge action. The latter would enable the identification of both the energy dissipation through the anticipated hysteresis of the materials and the exclusion of complete collapse of individual piers upon reaching maximum resistance and ductility.

In the framework of NLDA, two main input seismic motions were further defined (two more configurations to add to scenarios n. A and B defined above in Section 3): n. 1 is based on a spectrum-compatible accelerograms approach, and n. 2 is based on a site-specific and spectrum-compatible accelerograms experimental approach.

Starting from configuration n. 1, for the selection of accelerograms for local seismic response studies, reference is made to the work of Iervolino et al. [48] and the Rexel software [48] where the geographical position and the site parameters serve as inputs (Long. 10.011, Lat. 44.627, soil type A, T_2 topography, Class IV, SLV), and disaggregation analysis was subsequently carried out within the software itself. Following the procedure suggested in [49], we arrive at the graph in Figure 6 which illustrates the results of the disaggregation analysis in terms of a three-dimensional graph representing the contribution of the seismogenic sources placed at a distance R and capable of generating an earthquake of magnitude M to be the source of an earthquake that dominates the site scenario [50]. It is evident from Figure 6 that the most significant contribution to hazard was due to seismogenic sources within a radius of 20 km with magnitudes between 4.0 and 6.0. Therefore, the accelerogram selection process was carried out using Rexel and assuming the European Strong Motion catalogue as the starting database (Table 4).

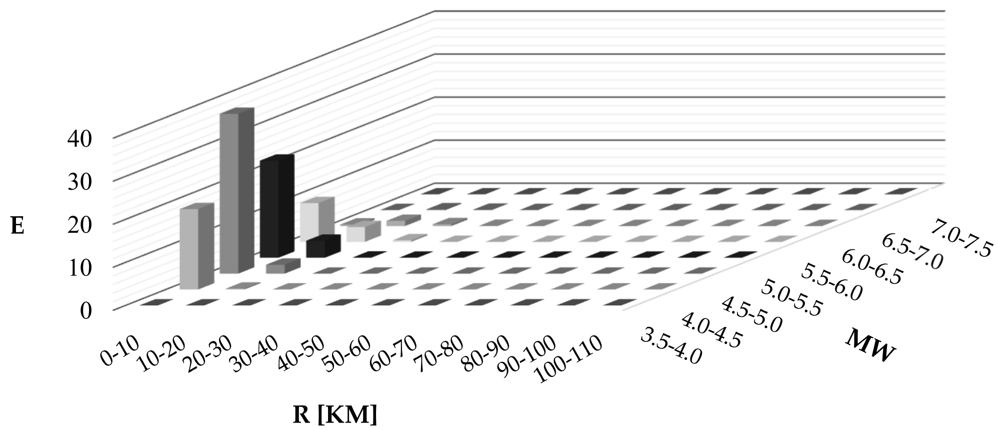

Figure 6. Illustration of the seismic hazard disaggregation, where the percentage contribution to the hazard estimate provided by all possible pairs of magnitude and distance values for a return period of 2475 years is highlighted.

Table 4. Selected accelerograms, providing evidence (underlined) of the main and minor events. * Emersito Seismic Network for Site Effect Studies in L'Aquila town, ** Italian Strong Motion Network (RAN).

Signal Source	Station Code	Nation	Event	Mw	Epicentral Location	Epicentral Distance [km]	PGA [g]
ESSEA *	MI05	Italia	7 April 2009 17:47	5.5	Fossa (AQ)	3.6	0.66
DPC **	MMO	Italia	30 October 2016 06:40	6.5	Norcia (PG)	19.3	0.19
DPC **	BSC	Italia	23 November 1980 18:34	6.9	Laviano (SA)	28.3	0.09
DPC **	CLO	Italia	26 October 2016 19:18	5.9	Visso (MC)	10.8	0.22
DPC **	LSS	Italia	24 August 2016 01:36	6.0	Accumoli (RI)	26.7	0.02
DPC **	MTR	Italia	6 April 2009 01:32	6.1	L'aquila (AQ)	23.1	0.06
DPC **	VGG	Italia	9 September 1998 11:28	5.6	Laino Borgo (CS)	2.5	0.08

Moving to configuration n. 2, since the purpose of this research paper is to conduct dynamic analyses on the motorway viaduct, the derivation of a new set of accelerograms compatible with the site-specific spectrum derived from local seismic response analyses is needed. For this purpose, Seismomatch® [51], a well-known software specialized in the selection and treatment of seismic signals preparatory to structural analyses, was used. The basis for the spectrum compatibility for both directions will be the response spectrum in normalized form. Figure 7 reports the matched spectra for the MTR station in the X direction.

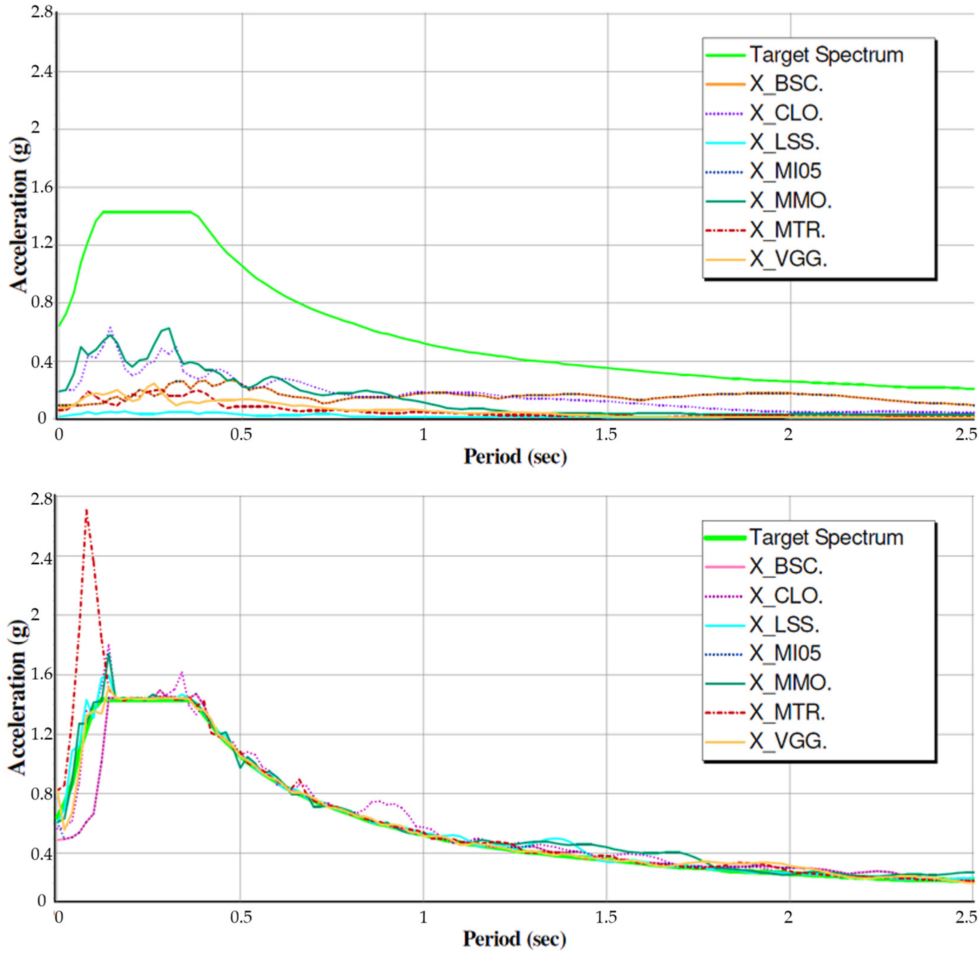

Figure 7. Response spectra of the selected accelerograms in Table 4 in X direction (**upper**) and the respective matching response spectra (**lower**).

4. Numerical Model of Structural Components and Details

To investigate the seismic response of the case study viaduct, the variables considered are mainly related to the following combination of real situations:

- the increase in seismic loads due to the presence of traffic (scenario A and scenario B);
- the presence of appreciable local seismic phenomena (config. n. 1 NSS and config. n. 2 SS)

Eight different numerical models are outlined and then described. First, static and dynamic nonlinear analyses were carried out corresponding to the different cases identified according to the configurations depicted in Figure 8 [52,53].

Type of analysis	Seismic INPUT	Traffic Load Scenario
NLDA	NSS	A
NLDA	NSS	B
NLDA	SS	A
NLDA	SS	B
NLSA	NSS	A
NLSA	NSS	B
NLSA	SS	A
NLSA	SS	B

FEM ANALYSIS Configuration n°
1. NLDA ->NSS -> A
2. NLDA ->NSS -> B
3. NLDA ->SS -> A
4. NLDA ->SS -> B
5. NLSA ->NSS -> A
6. NLSA ->NSS -> B
7. NLSA ->SS -> A
8. NLSA ->SS -> B

Figure 8. Comparative configurations of the analysis strategies undertaken.

The initial properties of the materials were taken from the calculation report available, considering unitary confidence factors tabulated in the Italian code as a function of the knowledge levels acquired based on the results of specific in-situ tests and inspections [54,55]. The choice of the constitutive laws of the steel and concrete materials is of fundamental importance as it will significantly influence the structural behaviour. The stress-deformation response of the materials governs the behaviour of all elements (beams, piles and load-bearing system). One of the characteristics that most affects the behaviour of concrete is the presence or not of transverse reinforcement (stirrups/shear reinforcement) which, as is known, in addition to improving the axial load capacity of the single beam/column, also improves its ductility. To capture this phenomenon, the constitutive bond proposed by Kent and Park [56] for concrete was adopted, referring to the behaviour of the material in compression and neglecting the contribution of tension.

The purpose of this research is to investigate the overall earthquake effects on the bridge. For this reason, the choice of modelling the viaduct entirely with one-dimensional beam elements seems reasonable. A lumped mass model approach was used. Indeed, the geometry of the piles considered the two main elements that compose it: the pier and the header (or pier cap). The pier, made up of two side-by-side partitions, was represented as rectangular sections, as per the design geometry. The two beam elements were then connected at the head by a coupling beam. The critical challenge to reflect the complex geometry of the header with a good degree of approximation was overcome by using "tapered" geometry as indicated in Figure 9.

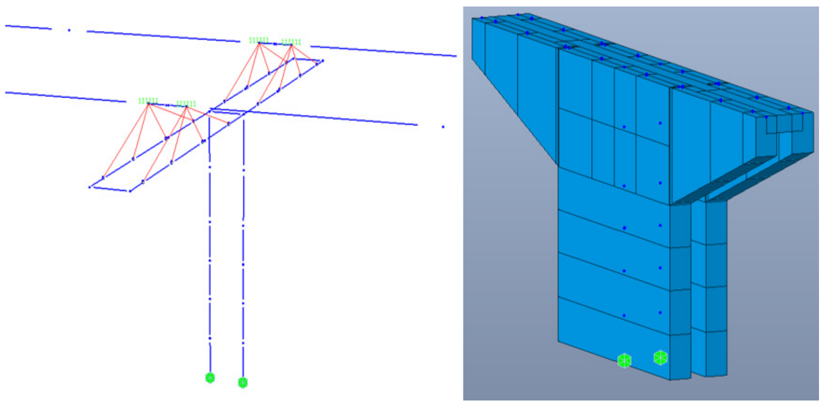

Figure 9. Finite element model of the pile-type using tapered beams where "rigid-links" are illustrated and modelled to simulate the real distance between the barycentric longitudinal axis of the deck and the neoprene support on the pulvinus.

The choice of nodal lumped mass assignment leads inevitably to allocating a portion of the pile mass to the base joint node, which cannot be mobilized to contribute to the seismic inertial forces. Therefore, if the pile was modelled with a single beam element, half of the mass of the single pile would be discarded. To mitigate this effect, the pile shaft has been discretized into multiple beam elements, not exceeding a length of 1 m each.

At the base of the pile, fully fixed constraints were considered: this assumption was considered valid due to the order of magnitude of the rigidity of the shaft foundations concerning the piers. The deck was also modelled with linear beam-like elements and using Midas® Gen's SPC (Section Property Calculator) tool, the prestressed beams and the slabs were both considered part of the same section of the beam: the centre of gravity of the beam is therefore considered to be the centre of gravity of the entire "complex" section (Figure 10a). The complete modelling of the case study bridge deck is illustrated in Figure 10b,c.

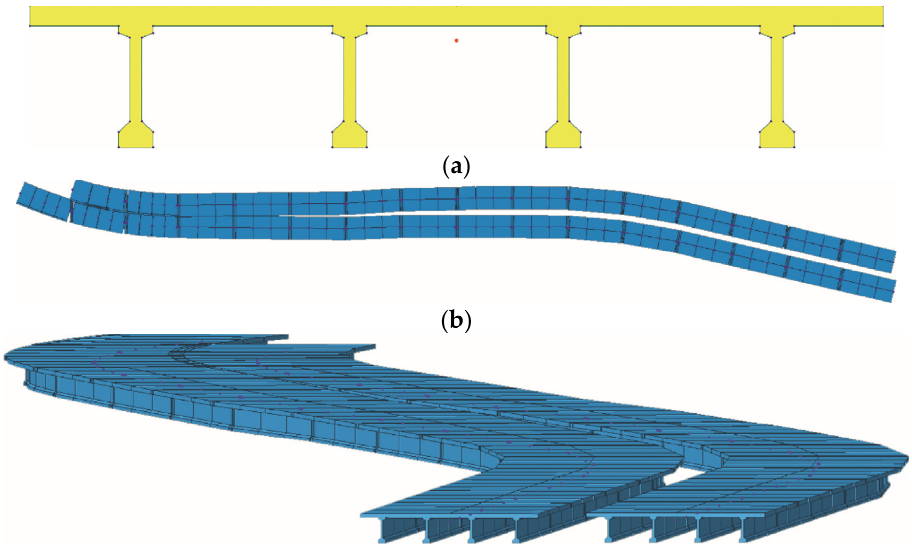

(**a**)

(**b**)

(**c**)

Figure 10. (**a**) Illustration of the beam element model of the bridge deck. (**b**) Plan view of the deck finite element model. (**c**) Perspective view for deck finite element model.

The reinforced neoprene supports have been modelled as a "general link" of the "spring" type. The element has five degrees of freedom (DOF) considering that the rotation (torsion) around its local vertical barycentric axis (X) was not included in the model. The other translational and rotational stiffnesses were calculated based on the reference literature for the "elastomeric bearings" (UNI EN 1337-3, 2005), of which a summary is reported in Table 5. In the real structure, all the prestressed beams are placed directly on the reinforced neoprene supports positioned on the top of the piles. Under the hypothesis made to consider only one beam element per carriageway, this criticality was resolved with the use of "rigid links", attributing the "master" property to the node on the girders, and "slave" to the four support points on the stack.

Table 5. Stiffness parameters of neoprene supports.

Kv (vertical stiffness along X-axes)	1,533,877	N/mm
Kh (horizontal stiffness, X and Y plane)	2857	N/mm
Kα,x (bending stiffness about X-X axes)	19.8×10^9	Nmm
Kα,y (bending stiffness about Y-Y axes)	35.2×10^{10}	Nmm

It was decided to insert non-structural elements, such as highway barriers and connecting crosspieces of beams, only as nodal point loads [57]. In addition to the latter and the structural self-weights, the load of the flooring was modelled as a linear load applied to the deck beams. Overall, the unloaded bridge model ("scenario A") with only the permanent loads and loads of the non-structural element applied, appears as shown in Figure 11.

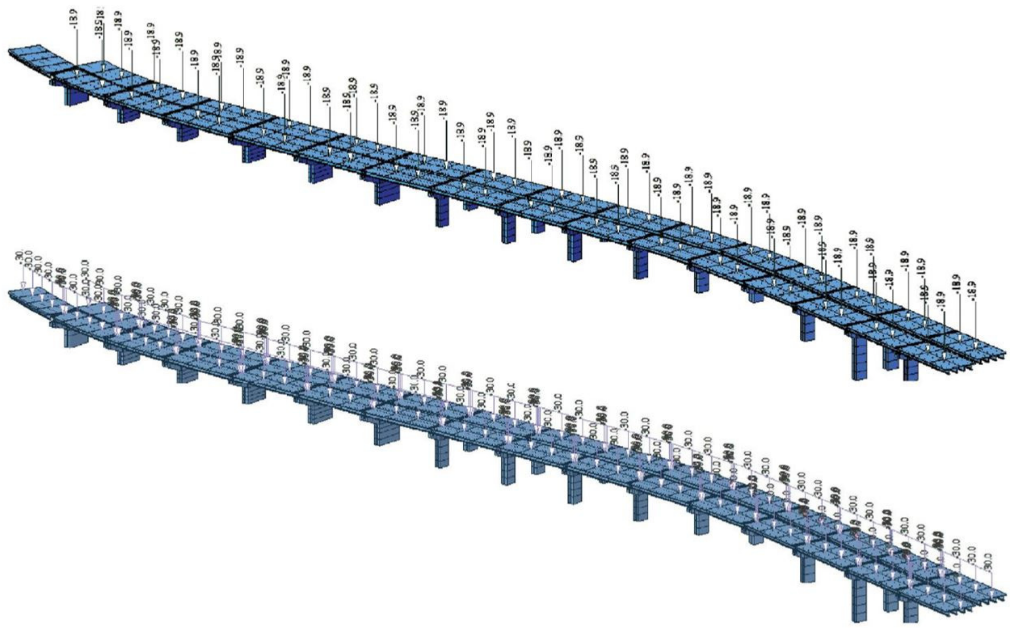

Figure 11. Nodal loads from non-structural elements (**upper**) and pavement linear loads (**lower**).

To summarize, the RC sections of the bridge (i.e., piles, piers, pre-stressed beams, and deck) were modelled solely with beam finite elements. The neoprene bearing elements of the beams on the piers were modelled with "general-link" elements in MidasGen, where the stiffness matrix elements which were calculated with reference to the simplified UNI 1337-3 method were manually inserted. The deck was modelled with a single beam element, and the section imported from SPC is shown in Figure 10a. To simulate the actual support of the prestressed RC beams on their respective neoprene bearings, "rigid-link" elements were used to account for the vertical eccentricity.

To obtain the vibration modes of the complex bridge structure, an eigenvalue analysis was performed. To do this, as a preliminary step, an estimation of the stiffness of the piles in the cracked phase was taken into account. Method 1 "of effective inertia" proposed in Eurocode 8 [58] was applied, which is briefly reported below:

$$J_{eff} = 0.08 \cdot J_{un} + J_{CR}$$

$$J_{CR} = \frac{M_y}{(E_c \cdot \chi_y)}$$

where J_{un} is the moment of inertia of the gross section of the uncracked pier, J_{CR}, is the moment of inertia of the cracked section at the yield point of the tensile reinforcement; M_y and χ_y are the yield moment and curvature of the section, respectively; and E_c is the elastic modulus of concrete. Therefore, the critical stiffness will depend on the moment–curvature diagrams of the piles (and consequently also on the static axial load of the single pile). From these considerations, an average reduction of the non-cracked inertia of about 80% was applied to the piles, which was managed in Midas® Gen through the combined use of the "stiffness scale factor" command and the "boundary change assignment". The first was used to create the case of modified inertias with the cracked phase, whereas the latter was used to separately manage the static analysis (conducted with the original elastic stiffnesses) and the eigenvalue analysis and all subsequent descending considerations on the seismic response (conducted for the cracked phase).

To include a significant percentage of the viaduct mass (not less than 85%, according to [41]), the modal analysis had to involve a very high number of modes. This is because the high-frequency modes make considerable contributions to the overall response. For these reasons, it was decided to carry out an analysis with Ritz vectors considering two horizontal forcings at the base in the two directions X and Y and calculating a subspace of m = 30 Ritz vectors for the "n" unknowns of the eigenvalue problem [59]. Table 6 reports a comparison between the modal analysis and the analysis with Ritz vectors in which the mass contribution is around 97 and 90% corresponding to the X and Y directions, respectively, attained considering 30 modes. The information gathered by comparing the calculated modes using two different techniques and the overall consistency of modal displacements and periods provides useful insights into the validation of the FEM model and the soundness of the approach taken.

Table 6. Summary of the results obtained for the modal analysis and the Ritz eigenvalues.

Mode N°	MODAL ANALYSIS						RITZ EIGENVALUES			
	X-DIR		Y-DIR		T (s)	T (s)	X-DIR		Y-DIR	
	MASS (%)	SUM (%)	MASS (%)	SUM (%)			MASS (%)	SUM (%)	MASS (%)	SUM (%)
1	9.74	9.74	0.40	0.40	1.36	1.36	9.74	9.74	0.40	0.40
2	25.67	3.,41	0.00	0.40	1.32	1.32	25.67	35.41	0.00	0.40
3	7.81	43.22	0.34	0.73	1.23	1.23	7.81	43.22	0.34	0.73
4	8.41	51.63	0.00	0.74	1.19	1.19	8.41	51.63	0.00	0.74
5	2.38	54.01	0.01	0.74	1.10	1.10	2.38	54.01	0.01	0.74
6	8.57	62.58	0.01	0.75	1.07	1.07	8.57	62.58	0.01	0.75
7	2.87	65.45	0.01	0.76	0.98	0.98	2.87	65.45	0.01	0.76
8	3.00	68.45	0.04	0.80	0.92	0.92	3.06	68.50	0.04	0.80
9	0.56	69.01	0.00	0.80	0.91	0.90	0.63	69.13	0.00	0.80
10	0.22	69.23	5.53	6.33	0.89	0.89	0.24	69.37	6.05	6.85
11	0.10	69.33	0.00	6.34	0.89	0.89	0.16	69.53	4.56	11.41
12	0.20	69.52	5.03	11.36	0.89	0.86	6.78	76.31	0.05	11.45
13	6.58	76.10	0.06	11.42	0.86	0.81	0.00	76.31	11.50	22.96
14	0.06	76.16	0.06	11.49	0.85	0.80	4.06	80.37	0.01	22.97
15	0.05	76.21	0.02	11.51	0.83	0.78	0.08	80.46	9.17	32.14
16	0.06	76.27	0.06	11.56	0.83	0.76	4.17	84.62	0.12	32.26
17	1.03	77.29	0.13	11.69	0.81	0.74	0.05	84.68	30.35	62.61
18	0.14	77.43	11.63	23.33	0.81	0.72	1.75	86.43	0.55	63.16
19	1.64	79.07	0.15	23.48	0.80	0.71	0.09	86.52	6.07	69.22
20	0.86	79.93	0.01	23.49	0.79	0.54	0.01	86.52	0.12	69.34
21	0.16	80.09	0.83	24.31	0.79	0.48	0.00	86.53	0.06	69.41
22	0.02	80.11	6.52	30.83	0.79	0.43	0.12	86.64	0.00	69.41
23	0.73	80.84	0.27	31.10	0.78	0.35	0.52	87.16	0.02	69.43
24	0.62	81.46	0.01	31.12	0.77	0.34	1.39	88.55	0.00	69.43
25	0.03	81.49	0.30	31.42	0.77	0.28	2.48	91.04	0.03	69.46
26	2.15	83.64	0.05	31.47	0.76	0.24	0.10	91.14	1.15	70.61
27	0.24	83.88	0.01	31.48	0.76	0.19	1.90	93.04	0.11	70.71
28	0.01	83.89	1.13	32.62	0.75	0.15	0.05	93.09	7.10	77.81
29	0.02	83.92	0.28	32.90	0.74	0.08	4.10	97.19	0.08	77.89
30	0.02	83.94	0.09	32.99	0.74	0.07	0.08	**97.26**	12.20	**90.09**

Figures 12 and 13 show a qualitative representation of modal displacement for the first two main modes in the two directions. The slender pile (Pile 14 South) immediately activates the main mode in the X direction with a proper period of 1.34 s (Figure 12a). An example of higher modes is illustrated in the following figures, in the X-direction (Figure 12b) and Y-direction (Figure 13a,b).

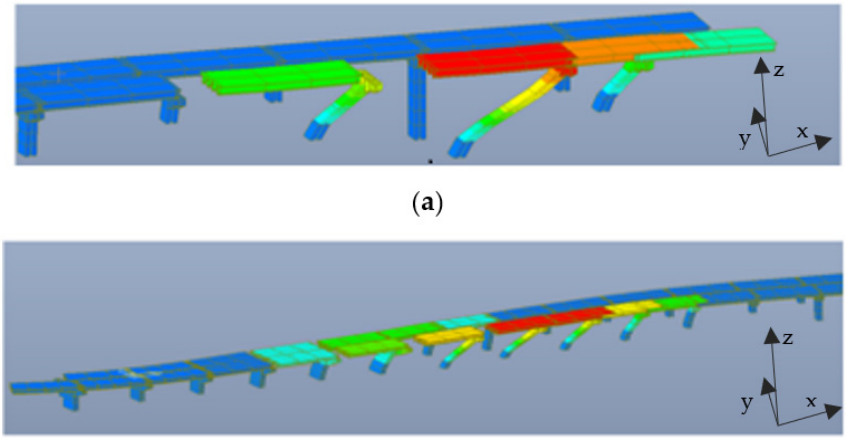

(**a**)

(**b**)

Figure 12. (**a**) First mode X-direction (pile 14S). (**b**) Second mode X-direction (south piles of the central sector of the bridge).

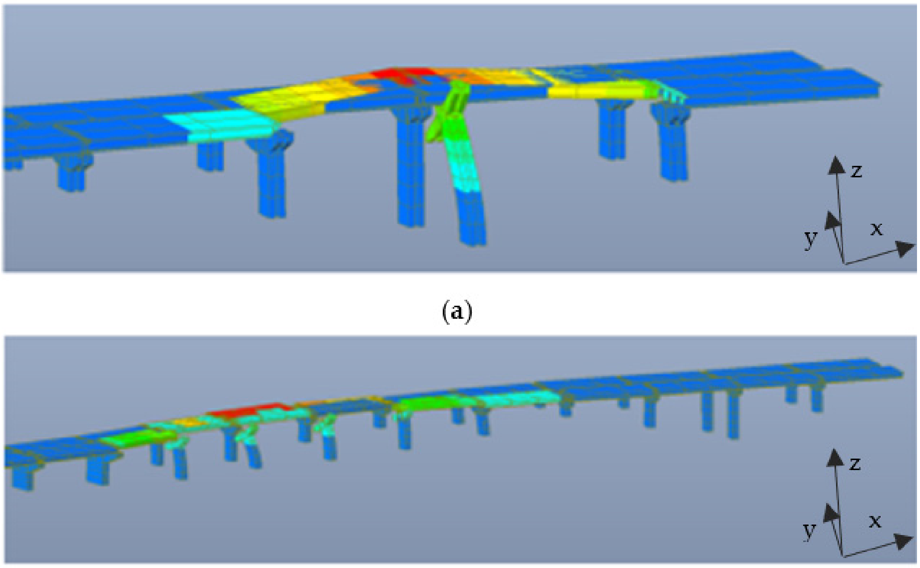

(**a**)

(**b**)

Figure 13. (**a**) Tenth mode Y-direction (pile 14S). (**b**) Thirteenth mode Y-direction (south piles of the central sector of the bridge).

To proceed with the subsequent calculation step, the introduction of nonlinearity to the numerical model is required. Therefore, a concentrated/lumped plasticity hinge model was adopted, whose characteristics are calibrated according to the effective resistance and rotational capacities derived from the individual moment–curvature diagrams [60]. The steel reinforcements used for the derivation of the moment–curvature diagram were derived from a simulated project benefiting from historical data on materials present in the literature [61]. Only the ductile mechanism was considered, characterized by force–displacement curves in which it is possible to find an elastic phase and a subsequent and distinguishable post-elastic hardening phase. The goal is to capture the most significant general aspects of the viaduct's flexural capacity. To do this, it was necessary to model the plastic hinges, the area in which the rotation of the shaft was expected to concentrate and in which the structural damage would be concentrated. Operationally, the following steps were performed:

- calculation of the moment–curvature of the single pile subjected to the design axial load;
- definition of an idealized bilinear constitutive element link;
- evaluation of the "coordinates" (M-χ) of the yield and failure points of the section;
- conversion of curvatures into rotations through the integration along the length of the plastic hinge with the equations commonly available in the literature [62]

$$\theta_y = L_{pl} \cdot \chi_y$$
$$\theta_u = L_{pl} \cdot \chi_u$$
$$L_{pl} = 0.1L_v + 0.17h + 0.24\frac{d_{bl} \cdot f_y}{\sqrt{f_c}}$$

where d_{bl} is the diameter of the longitudinal tensile reinforcement, f_y is the yield stress of the steel, f_c is the compressive strength of the concrete, h is the height of the section and L_v is the "shear span" defined as the distance to the inflection point of the member.

5. Multi-Modal Pushover Analysis (MMPO)

With reference to load scenario A, we focused on the manual calculation of the seismic vulnerability index (*IV*) of the 14 southern pile in the X direction (of lower inertia) which, with its 14.09 m, is the highest. The verification carried out starting from the reference response spectrum (RS) in Figure 2 was not satisfied. Therefore, we proceeded by trial and error, scaling the reference spectrum (Figure 14) for the seismic action that determines the Performance Points (PP) on the individual capacity curves with a multiplication factor of 1/q.

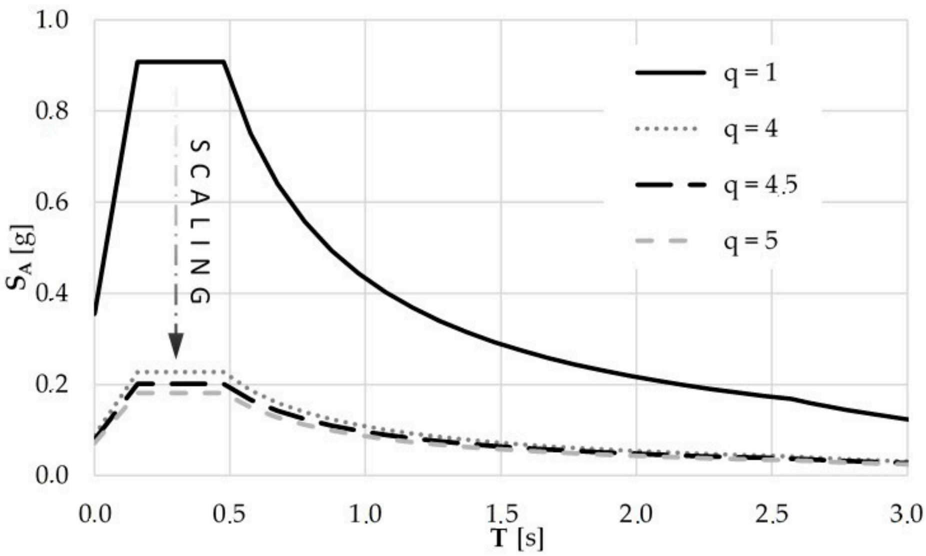

Figure 14. Scaling process of load response spectrum (elastic-Vr of 200 years, soil type C, T 2 h/H of 0.5) for multi-modal pushover analysis method.

The value of q = 4.5 approximated relatively well to the limit condition at the life safety limit state for the 14S pile, resulting in 99% of its maximum residual capacity in terms of the resisting moment (Table 7). Since 4.5 is a major parameter for the scale factors that allow the satisfaction of the SLV verification in favour of safety, the seismic vulnerability index (*IV*) in terms of V_{PGA} may be calculated as:

$$IV - V_{PGA} = \frac{a_{SLV}}{a_{g,SLV}} = \frac{\frac{0.355}{4.5}}{0.355} = \frac{1}{4.5} = 0.22$$

Table 7. Trial and error iterative safety check. Limit-seismic input for response spectrum scaled for q = 4.5.

q	M_{ed}	$M_{ultimate,d}$	M_{Rd} (0.75 × $M_{Ultimate,d}$)	ULS Safety Check (Mrd > Med)	M_{ed}/M_{rd} (Sectional Safety Factors)
5	1655	2445	1834	OK	0.90
4.5	1815	2445	1834	OK	0.99
4	1990	2445	1834	**NOT VERIFIED**	**1.08**

The 14S pile, therefore, could withstand just 22% of the project seismic action at the SLV. However, this did not provide us with information on the overall performance of the viaduct which, although damaged, under the dissipative areas identified by the plastic hinges (Figure 15), could withstand a greater seismic action as a whole.

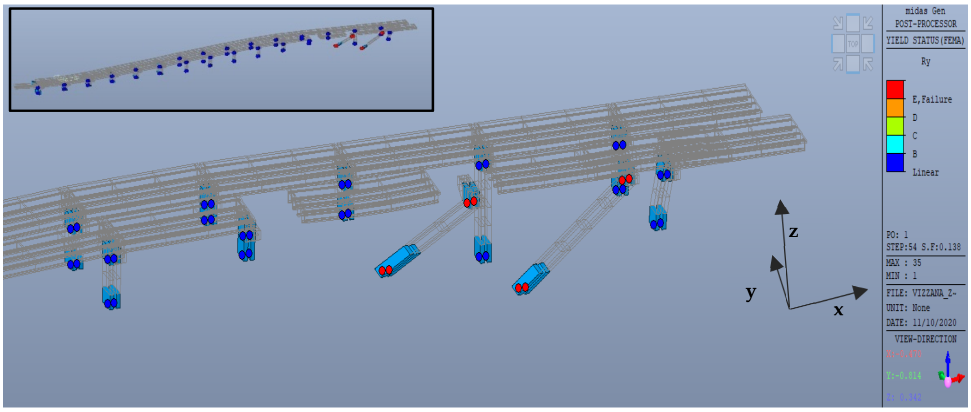

Figure 15. Example of displacement of northern piles 13 (**left**) and 14 (**right**) at step 54 for pushover curve n. 1 (main period).

In load scenario B, the stresses were better distributed over the entire viaduct and consequently, the South pile 14 was less stressed. Indeed:

$$IV - V_{PGA} = \frac{a_{SLV}}{a_{g,SLV}} = \frac{\frac{0.643}{0.95}}{0.643} = \frac{1}{1.73} = 1.05$$

In this condition, therefore, the 14 southern pile X direction verified the safety condition. Table 8 summarises the results of the safety check following the application of the multi-modal approach. The SS input condition for the non-overloaded deck (load A) resulted in a higher vulnerability of southern pile 14.

Table 8. Nonlinear static analysis (NLSA) configuration with MMPO approach—pile 14S X-dir. check (vulnerability index). Unsatisfied verifications are highlighted in bold, worst condition is underlined.

	IV-V_{PGA}	
	Scenario A	Scenario B
NSS	**0.22**	1.05
SS	**0.12**	**0.58**

6. Time-History Analysis

Seven nonlinear time history analyses were carried out using the seven selected accelerograms, averaging—for the calculation of the stresses—the unfavourable results on the conducted time-histories as required by the Italian NTC 2018. In addition to the structural safety check, it is of interest to this study to understand which piles were most affected by the dynamics of the seismic event.

To properly understand this aspect, the damage to the individual piers of the viaduct at the end of each time history in the two vertical loading scenarios (A without traffic load, B with traffic load included) was analyzed according to the FEMA plastic hinges criterion. Regarding the ultimate limit state (ULS) check, the bending moments were extracted from the FEM model calculation, averaged from the time histories and compared with the resistant moments according to FEMA criterion.

There was substantial compliance with the life safety limit state in the NSS approach (Table 9). By contrast, due to the much more amplified nature of some accelerograms based on a site-specific (SS) spectral matching, the damage reported for the viaduct was more significant (Table 9). Concerning the force verification, however, it is noted that in the direction of the weak axis (X direction), the verifications were satisfied for both load scenarios and both NSS and SS approaches. On the other hand, around the strong axis, some verifications were deemed non-compliant, with many elements remaining unverified and the slightly worse scenario B.

Table 9. Piles check (safety factors). Nonlinear dynamic analysis (NLDA) combined with non-site-specific (NSS) and site-specific (SS) approaches. Safety conditions were satisfied for all piles with regards to NSS approach. Unsatisfied verifications are in bold and worst condition is underlined in SS approach.

	NLDA –> NSS				NLDA –> SS			
	X-DIR		Y-DIR		X-DIR		Y-DIR	
Pile n°	**Scenario A**	**Scenario B**	**Scenario A**	**Scenario B**	**Scenario A**	**Scenario B**	**Scenario A**	**Scenario B**
1	20.54	1.89	215.80	5.79	3.62	3.84	66.98	66.98
2	2.13	3.46	4.45	9.25	1.00	1.15	1.41	1.13
3	2.31	2.85	4.57	7.23	1.09	1.31	1.33	1.07
4	2.21	3.03	4.42	7.50	1.03	1.27	1.33	1.07
5	2.25	3.00	4.99	6.80	1.05	1.31	1.45	1.16
6	2.51	6.18	5.64	14.89	1.18	1.44	1.70	1.43
7N	2.46	2.67	2.69	2.69	1.22	1.31	**0.97**	**0.85**
7S	2.23	2.70	2.31	2.75	1.14	1.37	**0.93**	**0.86**
8N	2.80	2.69	2.14	2.74	1.36	1.43	**0.92**	**0.83**
8S	2.58	2.78	2.49	2.63	1.27	1.36	**0.96**	**0.91**
9N	2.67	2.78	2.99	2.63	1.33	1.38	1.06	**0.90**
9S	2.60	3.05	2.41	2.88	1.32	1.37	**0.97**	**0.90**
10N	2.78	3.05	3.43	2.89	1.34	1.39	1.09	**0.95**
10S	2.66	3.42	2.37	3.99	1.29	1.34	**0.95**	**0.87**
11N	2.63	3.42	2.86	4.03	1.30	1.35	**0.95**	**0.83**
11S	3.08	4.09	2.79	7.97	1.38	1.43	1.01	**0.89**
12N	2.81	3.96	4.41	7.78	1.21	1.44	1.23	1.08
12S	2.76	3.06	4.42	3.62	1.22	1.41	1.30	1.10
13N	2.83	3.18	4.54	3.66	1.36	1.42	1.20	1.10
13S	2.89	3.86	3.08	2.20	1.35	1.43	1.07	**0.95**
14N	3.32	4.04	2.13	2.28	1.31	1.59	**0.91**	**0.87**
14S	2.96	3.32	2.14	4.31	1.29	1.56	**0.92**	**0.87**
15N	2.77	3.17	3.43	4.25	1.32	1.39	1.08	**0.98**
15S	2.86	19.41	3.12	76.82	1.33	1.41	1.05	**0.95**

Regarding the site-specific (SS) and spectrum-compatible accelerogram experimental approach (scenario B), due to the nature of the amplified accelerograms based on a site-specific spectral matching as obtained above, the damage reported for the viaduct is highly significant. Across all performed time histories, in fact, the plastic hinges almost systematically indicate serious damage only in the Y direction, with slightly better behaviour in the scenario A load-condition.

7. Conclusions

The analyses conducted, and the comparison strategies introduced, showed a general consistency of results, and may be summarized as follow:

7.1. Multi-Modal Pushover Analysis

The multi-modal pushover analysis tool (MMPO) allows assessments on seismic vulnerability to be conducted even where, as in the case in question, a uni-modal nonlinear static analysis would be ineffective and unreliable.

When considering all the significant modes, it is possible to capture the general trend of the structural behaviour of the case study bridge as a whole without disregarding the effects of the higher modes. As such, the eigenvalue analysis with Ritz vectors facilitates the selection of significant modes by reducing the computational burden associated with time and effort. In general, it was observed that the results obtained with nonlinear static analysis (NLSA) are more conservative when compared to the results of dynamic analyses. While this penalizes the cost-effectiveness of a possible retrofitting or assessment intervention, it does not affect the reliability associated with the performed calculations even at a larger scale (i.e., regional scale).

7.2. Nonlinear Time-History Analysis

This is a greater cost and computational time-consuming analysis, but fewer conservative results are found compared to MMPO: a more accurate calculation model and analysis procedure lead to results that are most likely more realistic.

7.3. Local Seismicity Effects

It has been seen how the local seismicity of the site of interest strongly influences the seismic structural checks of the case study bridge. Nevertheless, with a simplified model, the expeditious forecasts derived from the geological studies of level 2 seismic micro-zoning on a municipal scale have been fully confirmed: the site-specific spectrum results in the range of periods between 0.1 s < T < 0.5 s amplified by a factor of about two (Figure 16). The amplification of the seismic action causes a predictable deterioration of the structural behaviour with severe damage spreading throughout the viaduct. In particular, it is highlighted how, by applying amplified accelerograms deriving from local-seismic-response (LSR) studies, structural checks are often not respected around the weak axis of the piles.

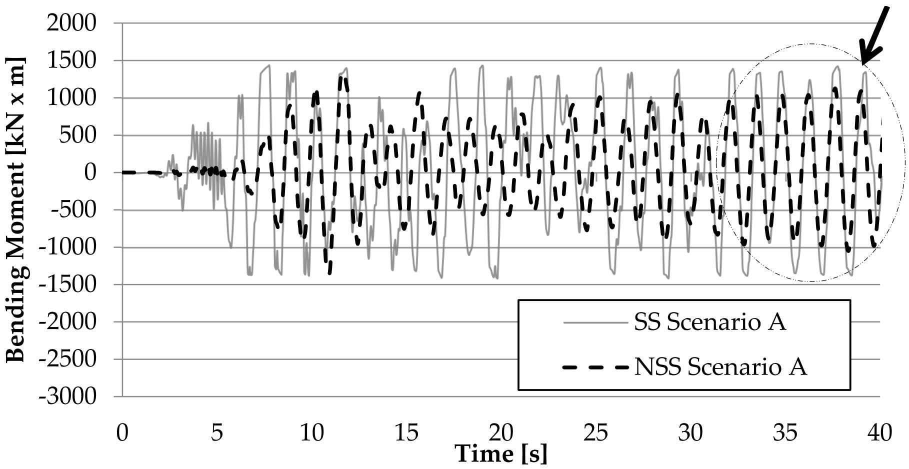

Figure 16. Comparison of moment My at the base of southern pile 14, time history BSC (Laviano)–load scenario A (unloading viaduct).

7.4. Traffic Load Effects

Despite the increase in seismic masses and therefore of the forces of inertia applied on the viaduct, the contextual increase in the proper periods due to the same increase in mass is predominant in the X direction (weak axis). Both the risk indices identified on the southern pile 14 in the MMPO and the capacity rates of the base sections identified in the nonlinear dynamic analysis (NLDA) are systematically better, passing from load scenario A (unloaded viaduct) to load scenario B (viaduct with traffic load). In general, there is also a redistribution effect of the seismic forces on all the piers, favoring the behaviour of the structure as a whole, and making it desirable to access the complete residual strength capacity (Figure 17). By contrast, in the Y direction (strong axis), we notice the opposite, with generally worsening behaviour from scenario A to scenario B. Overall, it can be said that the two load scenarios lead to the identification of different vulnerabilities of the individual piles and also changes the order in which the single piles plasticize first.

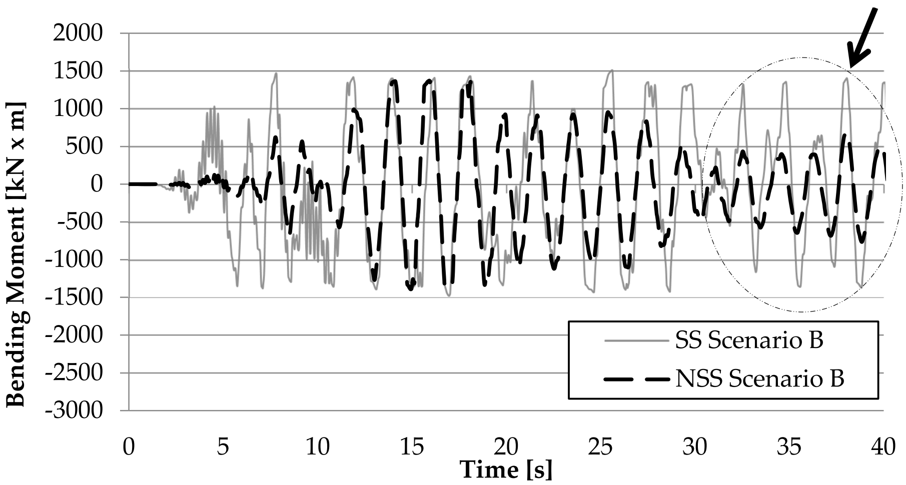

Figure 17. Comparison of moment My at the base of southern pile 14, time history BSC (Laviano)–load scenario B (with traffic load included).

7.5. Further Elements to Be Investigated

This study does not claim to exhaust all possibilities of further theoretical and practical study. In fact, of particular interest would be the further application of the MMPO procedure to all pier elements. Additionally, implementing a brittle shear failure model and evaluating its impact on the overall ductility of the structural system could be further investigated. At the same time, these results could be compared with NLDA results: in this way, the progressive damage of the viaduct could be evaluated in the event of a progressive brittle collapse of the most vulnerable piles. Moreover, a beneficial practical aspect would be the investigation of the kinematics of the viaduct through the modelling of "gap-elements" between the decks, which would consist of step-wise dynamic analyses including mechanisms such as the pounding and collapse of the beams due to loss of support. Since many structural checks with site-specific models of seismic actions are not respected, it would at least seem necessary to better examine this possibility. Specifically, in addition to the surface amplification of the seismic waves due to local stratigraphic effects, the possibility that the viaduct could also be subject to the spatial effect of the seismic motion due to geotechnical heterogeneity was excluded in the present study throughout its development (due to lack of access to specific investigations). In this sense, the possible beneficial effect of the soil-structure-interaction (SSI) on the stresses of the piles was not considered, and instead assumed in favour of safety for the entire structure, to apply constraints of perfect interlocking at the base. In any case, if further geognostic investigations and more refined studies of LSR (2D, 3D) were to confirm the amplified entity of the seismic action at the base, the opportunity to replace the old support devices to dynamically isolate the viaduct from the piers could be evaluated, a consolidation strategy that is currently generally minimally invasive and relatively cheap in its application. Finally, it would be fundamental to investigate the methods of energy dissipation by analyzing the general balance and the hysteresis of the structural elements through the elastic–plastic bonds of the hinges.

In conclusion, drawing definitive assumptions for the seismic behaviour of RC viaducts, particularly for bridges with multiple and lengthy spans, as analyzed in this article, is complicated. Such results depend heavily on the analysis strategy and seismic input choices, which may impact the costs associated with retrofitting strategies.

Additionally, the need to consider higher modes in the calculation of contributions to seismic stresses in nonlinear static analyses was demonstrated in this study. Neglecting the contribution of higher modes would result in a significant underestimation of the base action on the piles and overly optimistic conclusions. The multimodal approach in RC viaducts allows for accounting for these effects at the cost of significant computational effort, which could be implemented in automated routines using dedicated software. The application of this method is a natural tangible development of the theories formulated in [63], and appears as a further experimental step with respect to the recent applications in [64]. Such a routine, if appropriately implemented and calibrated, could represent a valid tool for calculating and validating results including for large and strategically important structures. From this perspective, it may be more advantageous to utilize the MMPO approach for smaller bridges, as it can deliver both speedy and reliable results.

The work also clearly highlighted that neglecting local effects could have a severe impact on the verification and design process of seismic retrofit interventions for highway viaducts. In areas susceptible to localized amplifications, due to the contribution of higher modes, this can lead to incorrect assessments of the vulnerability of the viaduct. Investing in geophysical and geotechnical surveys is therefore a wise choice and financial commitment for public administrations interested in safeguarding and protecting strategic infrastructure and human life. It could be shown in future work how such an initial investment automatically results in reduced maintenance costs, work times, and usability of the structure in the event of a seismic event.

Author Contributions: Conceptualization, methodology, software modelling and analysis, D.C.; investigation, resources, data curation, R.N.; writing—original draft preparation, writing—review and editing, D.C. and R.N. All authors have read and agreed to the published version of the manuscript.

Funding: This research received no external funding.

Institutional Review Board Statement: Not applicable.

Informed Consent Statement: Not applicable.

Data Availability Statement: Not applicable.

Conflicts of Interest: The authors declare no conflict of interest.

References

1. Kawashima, K.; Takahashi, Y.; Ge, H.; Wu, Z.; Zhang, J. Reconnaissance report on damage of bridges in 2008 Wenchuan, China, earthquake. *J. Earthq. Eng.* **2009**, *13*, 965–996. [CrossRef]
2. Pang, Y.; Cai, L.; Zhong, J. Seismic performance evaluation of fiber-reinforced concrete bridges under near-fault and far-field ground motions. *Structures* **2020**, *28*, 1366–1383. [CrossRef]
3. Xiang, N.; Goto, Y.; Alam, M.S.; Li, J. Effect of bonding or unbonding on seismic behavior of bridge elastomeric bearings: Lessons learned from past earthquakes in China and Japan and inspirations for future design. *Adv. Bridge Eng.* **2021**, *2*, 14. [CrossRef]
4. Salkhordeh, M.; Govahi, E.; Mirtaheri, M. Seismic fragility evaluation of various mitigation strategies proposed for bridge piers. *Structures* **2021**, *33*, 1892–1905. [CrossRef]
5. Wardhana, K.; Hadipriono, F.C. Analysis of recent bridge failures in the United States. *J. Perform. Constr. Facil.* **2003**, *17*, 144–150. [CrossRef]
6. Afsar Dizaj, E.; Salami, M.; Kashani, M. Seismic vulnerability analysis of irregular multi-span concrete bridges with different corrosion damage scenarios. *Soil Dyn. Earthq. Eng.* **2023**, *165*, 107678. [CrossRef]
7. Zucca, M.; Crespi, P.; Stochino, F.; Puppio, M.L.; Coni, M. Maintenance interventions period of existing RC motorway viaducts located in moderate/high seismicity zones. *Structures* **2023**, *47*, 976–990. [CrossRef]

8. Crisci, G.; Ceroni, F.; Lignola, G.P.; Prota, A. Critical issues in existing RC deck stiffened arch bridges under seismic actions. *Eng. Struct.* **2022**, *272*, 114980. [CrossRef]
9. Simanjuntak, V.C.; Imran, I.; Moestopo, M.; Setio, H.D. The Evolution of Seismic Design Provisions in Indonesia's National Bridge Code. *J. Eng. Technol. Sci.* **2022**, *54*, 220614. [CrossRef]
10. Wallace, J.W.; Eberhard, M.O.; Hwang, S.J.; Moehle, J.P.; Post, T.; Roblee, C.; Stewart, J.P.; Yashinsky, M. Highway bridges. *Earthq. Spectra* **2001**, *17*, 131–152. [CrossRef]
11. Yen, W.-H. Lessons learned about bridges from earthquake in Taiwan. *Fed. Highw. Adm.* **2002**, *65*, 20–23.
12. Imbsen, R.A.; Roblee, C.J.; Yashinsky, M.; Berilgen, M.M.; Toprak, S. Impact on highway structures. *Earthq. Spectra* **2000**, *16*, 411–435. [CrossRef]
13. Ghasemi, H.; Cooper, J.D.; Imbsen, R.; Piskin, H.; Inal, F.; Tiras, A. The November 1999 Duzce earthquake: Post-earthquake investigation of the structures. In *TEM. Publication No. FHWARD-00–146*; Federal Highway Administration: Washington, DC, USA, 2000. Available online: https://rosap.ntl.bts.gov/view/dot/41585 (accessed on 9 February 2023).
14. De Domenico, D.; Messina, D.; Recupero, A. Seismic vulnerability assessment of reinforced concrete bridge piers with corroded bars. *Strct. Conc.* **2023**. [CrossRef]
15. Hafsa, F. A comparative study of RC bridge for evaluation of seismic performance and retrofit technology. *Innov. Infrastruct. Solut.* **2021**, *6*, 44–50.
16. Malomo, D.; Scattarreggia, N.; Orgnoni, A.; Pinho, R.; Moratti, M.; Calvi, G.M. Numerical Study on the Collapse of the Morandi Bridge. *J. Perform. Constr. Facil.* **2020**, *34*, 04020044. [CrossRef]
17. Calvi, G.M.; Moratti, M.; O'Reilly, G.; Scattarreggia, N.; Monteiro, R.; Malomo, D.; Calvi, P.M.; Pinho, R. Once upon a Time in Italy: The Tale of the Morandi Bridge. *Struct. Eng. Int.* **2019**, *29*, 198–217. [CrossRef]
18. Scattarreggia, N.; Salomone, R.; Moratti, M.; Malomo, D.; Pinho, R.; Calvi, G.M. Collapse analysis of the multi-span reinforced concrete arch bridge of Caprigliola, Italy. *Eng. Struct.* **2022**, *25115*, 113375. [CrossRef]
19. Ghazal, H.; Mwafy, A. Seismic fragility assessment of an existing multi-span RC bridge equipped with risk mitigation systems. *Buildings* **2022**, *12*, 982. [CrossRef]
20. Markou, G. A new method of seismic retrofitting cost analysis and effectiveness for reinforced concrete structures. *Eng. Struct.* **2021**, *2461*, 113083. [CrossRef]
21. Zanini, M.A.; Toska, K.; Faleschini, F.; Pellegrino, C. Seismic reliability of reinforced concrete bridges subject to environmental deterioration and strengthened with FRCM composites. *Soil Dyn. Earthq. Eng.* **2020**, *136*, 106224. [CrossRef]
22. Reggia, A.; Morbi, A.; Plizzari, G. Experimental study of a reinforced concrete bridge pier strengthened with HPFRC jacketing. *Eng. Struct.* **2020**, *2101*, 110355. [CrossRef]
23. De Domenico, D.; Sciutteri, S.; D'Arrigo, A.; Ricciardi, G. Seismic Retrofitting of Prestressed Concrete Bridges through Friction Pendulum Isolation Bearings. *Lect. Notes Civ. Eng.* **2022**, *200*, 604–612.
24. Di Sarno, L.; Paolacci, F. Experimental seismic assessment of the effectiveness of isolation techniques for the seismic protection of existing RC bridges. *Lect. Notes Civ. Eng.* **2017**, *2*, 89–114.
25. Nestovito, G.; Occhiuzzi, A. Implementation of smart-passive dampers combined with double concave friction pendulum devices to retrofit an existing highway viaduct exploiting the seismic early warning information. *Eng. Struct.* **2016**, *120*, 58–741. [CrossRef]
26. Cakebread, T. The role of finite element analysis in bridge assessment and design. In Proceedings of the 5th International Conference on Bridge Maintenance, Safety and Management, Philadelphia, PA, USA, 11–15 July 2010.
27. Duan, Y.F.; Xu, Y.L.; Fei, Q.G.; Wong, K.Y.; Chan, K.W.Y.; NI, Y.Q.; Ng, C.L. Advanced finite element model of TSING MA bridge for structural health monitoring. *Int. J. Struct. Stab.* **2011**, *11*, 313–344. [CrossRef]
28. Nguyen, V.T.; Achintya, J.H.; Hu, H.J. Fragility-based seismic performance assessment of modular underground arch bridges. *Structures* **2022**, *39*, 1218–1230.
29. Thapa, S.; Shrestha, Y.; Gautam, D. Seismic fragility analysis of RC bridges in high seismic regions under horizontal and simultaneous horizontal and vertical excitations. *Structures* **2022**, *37*, 284–294. [CrossRef]
30. Bandini, P.A.C.; Padgett, J.E.; Paultre, P.; Siqueira, G.H. Seismic fragility of bridges: An approach coupling multiple-stripe analysis and Gaussian mixture for multicomponent structures. *Earthq. Spectra* **2022**, *38*, 254–282. [CrossRef]
31. Franchini, A.; Sebastian, W.; D'Ayala, D. Surrogate-based fragility analysis and probabilistic optimisation of cable-stayed bridges subject to seismic loads. *Eng. Struct.* **2022**, *256*, 113949. [CrossRef]
32. Kildashti, K.; Makki Alamdari, M.; Kim, C.W.; Gao, W.; Samalia, B. Drive-by-bridge inspection for damage identification in a cable-stayed bridge: Numerical investigations. *Eng. Struct.* **2020**, *223*, 110891. [CrossRef]
33. Sebastian, W.M.; Johnson, M. Interpretation of sensor data from in situ tests on a transversely bonded fibre-reinforced polymer road bridge. *Struct. Health Monit.* **2019**, *18*, 1074–1091. [CrossRef]
34. Mengge, W.; Hao, Z.; Hongzhe, D.; Luming, S. A deep learning-aided seismic fragility analysis method for bridges. *Structures* **2022**, *40*, 1056–1064.
35. Minnucci, L.; Scozzese, F.; Carbonari, S.; Gara, F.; Dall'Asta, A. Innovative Fragility-Based Method for Failure Mechanisms and Damage Extension Analysis of Bridges. *Infrastructures* **2022**, *7*, 122. [CrossRef]
36. Collier, C.J.; Elnashai, A.S. A procedure for combining vertical and horizontal seismic action effects. *J. Earthq Eng.* **2001**, *5*, 521–539. [CrossRef]

37. Zhong, J.; Zhu, Y.; Han, Q. Impact of vertical ground motion on the statistical analysis of seismic demand for frictional isolated bridge in near-fault regions. *Eng. Struct.* **2023**, *278*, 115512. [CrossRef]
38. Karatzetzou, A.; Stefanidis, S.; Stefanidou, S.; Tsinidis, G.; Pitilakis, D. Unified hazard models for risk assessment of transportation networks in a multi-hazard environment. *Int. J. Disaster Risk Reduct.* **2022**, *751*, 102960. [CrossRef]
39. Yoon, Y.H.; Ataya, S.; Mahan, M.; Malek, A.; Abrahamson, N.; Zokaie, T.; Ong, R.; Ahmed, A. Total risk model and loss analysis of probabilistic damage control application in seismic design of highway bridges. *J. Bridge Eng.* **2022**, *27*, 04022020. [CrossRef]
40. Caigui, H.; Libo, C.; Leqia, H.; Weidong, Z. Comparative assessment of seismic collapse risk for non-ductile and ductile bridges: A case study in China. *Bull Earthq. Eng.* **2021**, *19*, 6641–6667.
41. NTC 2018–Norme Tecniche per le Costruzioni (NTC) Decreto Ministeriale, 17 January 2018 (In Italian). Ministero delle Infrastrutture e dei Trasporti, Rome, Italy. Available online: https://www.gazzettaufficiale.it (accessed on 12 February 2023).
42. Picinotti, P.F. *Relazione Illustrativa di Microzonazione Sismica del Comune di Terenzo*; Regione Emilia-Romagna: Terenzo, Italy, 2017. (In Italian)
43. Hashash, Y.M.A.; Musgrove, M.I.; Harmon, J.A.; Ilhan, O.; Xing, G.; Numanoglu, O.; Groholski, D.R.; Phillips, C.A.; Park, D. *DEEPSOIL 7, User Manual*; Board of Trustees of University of Illinois at Urbana-Champaign: Urbana, IL, USA, 2020.
44. Seed, H.B.; Idriss, I.M. *Soil Moduli and Damping Factors for Dynamic Response Analyses*; Technical Report; California University: Berkeley, CA, USA; Earthquake Engineering Research Center: San Francisco, CA, USA, 1970.
45. Newmark, N.M.; Hall, W.J. *Earthquake Spectra and Design*; Engineering Monographs, EERI: Oakland, CA, USA, 1982.
46. Romeo, R. Le azioni sismiche e le categorie di sottosuolo. *G. Di Geol. Appl.* **2007**, *6*, 65–80. (In Italian)
47. Liberatore, D.; Pagliaroli, A. Verifica della sicurezza sismica dei Musei Statali. Applicazione O.P.C.M. 3274/2003 s.m.i. e della Direttiva P.C.M. 12.10.2007. Convenzione Arcus–DG Rep. n. 113/2011 del 30/09/2011. Convenzione DG–Consorzio ReLUIS Rep. n. 21/2011 del 26/10/2011. Responsabile Scientifico: Domenico Liberatore. Referente Tecnico: Luigi Sorrentino (In Italian). Ministero della Cultura, Rome, Italy. Available online: https://www.beniculturali.it (accessed on 10 February 2023).
48. Iervolino, I.; Galasso, C.; Cosenza, E. REXEL: Computer aided record selection for code-based seismic structural analysis. *Bull. Earthq. Eng.* **2010**, *8*, 339–362. [CrossRef]
49. Iervolino, I.; Chioccarelli, E.; Convertito, V. Engineering design earthquakes from multimodal hazard disaggregation. *Soil Dyn. Earthq. Eng.* **2011**, *31*, 1212–1231. [CrossRef]
50. Cetraro, F. *Approccio Geotecnico Sugli Effetti Della Risposta Sismica Locale*; Flaccovio Editore: Palermo, Italia, 2019. (In Italian)
51. Seismosoft, "SeismoMatch–Verification Report". Available online: www.seismosoft.com (accessed on 10 January 2023).
52. Corritore, D.; Paolacci, F. Performance-based earthquake engineering analysis of short-medium span steel-concrete composite bridges. In Proceedings of the 8th International Conference on Computational Methods in Structural Dynamics and Earthquake Engineering, COMPDYN 2021, Athens, Greece, 28–30 June 2021. Code 174550.
53. Paolacci, F.; Giannini, R.; Alessandri, S.; Corritore, D. On the cyclic behaviour of new pier-to-deck connections for short-medium span composite I-girder bridges. *J. Traffic Transp. Eng.* **2018**, *5*, 439–453. [CrossRef]
54. Jalayer, F.; Elefante, L.; Iervolino, I.; Manfredi, G. Knowledge-Based Performance Assessment of Existing RC Buildings. *J. Earthq. Eng.* **2011**, *15*, 362–389. [CrossRef]
55. Ahmed, S.; Abarca, A.; Perrone, D.; Monteiro, R. Large-scale seismic assessment of RC buildings through rapid visual screening. *Int. J. Disaster. Risk Reduct.* **2022**, *80*, 103219. [CrossRef]
56. Kent, D.C.; Park, R. Flexural members with confined concrete. *J. Struct. Div.* **1971**, *97*, 1969–1990. [CrossRef]
57. Perrone, D.; Rodriguez, D.; Filiatrault, A.; Brunesi, E.; Beiter, C.; Piccinin, R. A Framework for the Quantification of Non-Structural Seismic Performance Factors. *J. Earthq. Eng.* **2022**, *26*, 8468–8494. [CrossRef]
58. Eurocode 8–Design of Structures for Earthquake Resistance—Part 2: Bridges. European Community, Bruxelles, Belgium. Available online: http://eurocodes.jrc.ec.europa.eu (accessed on 11 February 2023).
59. Leger, P.; Wilson, E.L.; Clough, R.W. *The Use of Load Dependent Vectors for Dynamic and Earthquake Analyses*; Earthquake Engineering Research Center report; University of California, Berkeley: Berkeley, CA, USA, 1986.
60. Crespi, P.; Franchi, A.; Giordano, N. Multimodal Pushover Analysis for R.C. Bridges. *Appl. Mech. Mater.* **2015**, *725*, 888–895. [CrossRef]
61. Verderame, G.M.; Stella, A.; Cosenza, E. Le Proprietà Meccaniche degli Acciai Impiegati nelle Strutture in Ca Realizzate negli Anni'60. In Proceedings of the X Congresso Nazionale L'ingegneria Sismica in Italia, Potenza-Matera, Italia, 9–13 September 2001.
62. Priestley, M.J.N.; Calvi, G.M.; Kowalsky, M.J. *Displacement-Based Seismic Design of Structures*, 2nd ed.; IUSS Press: Pavia, Italy, 2007; ISBN 88-85701-05-2.
63. Chopra, A.; Goel, R.K. A modal pushover analysis procedure for estimating seismic demands for buildings. *Earthq. Eng. Struct. Dyn.* **2002**, *31*, 561–582. [CrossRef]
64. Alici, F.S.; Sucuoglu, H. Practical Implementation of Generalized Force Vectors for the Multimodal Pushover Analysis of Building Structures. *Earthq. Spectra* **2014**, *31*, 1043–1067. [CrossRef]